International Journal of Solids and Structures 49 (2012) 1294–1303

Contents lists available at SciVerse ScienceDirect

International Journal of Solids and Structures

journal homepage: www.elsevier.com/locate/ijsolstr

Discontinuous bifurcation analysis in fracture energy-based gradient plasticity for concrete

S.M. Vrech [a], G. Etse [a,b,*,1]

[a] CONICET, National Council of Scientific and Technical Research, University of Tucuman, Alberdi 741, 4000 Tucuman, Argentina
[b] Department of Engineering, University of Buenos Aires, Maipu 780, 4000 Tucuman, Argentina

ARTICLE INFO

Article history:
Received 3 August 2011
Received in revised form 14 November 2011
Available online 18 February 2012

Keywords:
Gradient elastoplasticity
Geometrical failure analysis
Discontinuous bifurcation

ABSTRACT

Conditions for discontinuous bifurcation in limit states of selective non-local thermodynamically consistent gradient theory for quasi-brittle materials like concrete are evaluated by means of both geometrical and analytical procedures. This constitutive formulation includes two internal lengths, one related to the strain gradient field that considers the degradation of the continuum in the vicinity of the considered material point. The other characteristic length takes into account the material degradation in the form of energy release in the cracks during failure process evolution.

The variation from ductile to brittle failure in quasi-brittle materials is accomplished by means of the pressure dependent formulation of both characteristic lengths as described by Vrech and Etse (2009).

In this paper the formulation of the localization ellipse for constitutive theories based on gradient plasticity and fracture energy plasticity is proposed as well as the explicit solutions for brittle failure conditions in the form of discontinuous bifurcation. The geometrical, analytical and numerical analysis of discontinuous bifurcation condition in this paper are comparatively evaluated in different stress states and loading conditions.

The included results illustrate the capabilities of the thermodynamically consistent selective non-local gradient constitutive theory to reproduce the transition from ductile to brittle and localized failure modes in the low confinement regime of concrete and quasi-brittle materials.

1. Introduction

Quasi-brittle materials like concrete exhibit strong spatial discontinuities of the kinematic fields when they are sufficiently deformed into the inelastic regime. The formation of cracks and shear bands observed in experiments on concretes and soils are typical examples of localized failure mechanisms that strongly depend on the governing stresses and on the mechanical and chemical features of the material micro and mesostructure, see a.o. Vardoulakis (1980), Petersson (1981), Oda and Kazama (1988), Willam and Etse (1990), Ehlers and Volk (1997), van Mier (1997). In tensile regime the concrete response to mechanical loading is highly brittle as the damage entirely localizes in one single crack of zero width. Failure mechanism in tensile regime is fully controlled by the fracture energy release process in one single crack while the material outside the crack remains practically undamaged and subjected to elastic unloading, see a.o. Planas and Elices (1986), Planas and Elices (1989), Guo and Zhang (1987), Phillips and Binsheng (1993), Etse and Willam (1994).

In compressive regime the ductility of concrete failure behavior strongly increases with the confining pressure. The failure mechanism is characterized by both the appearance of several microcracks in the normal direction to the local maximum principal stress and by the evolution of material damage processes in zones located in between cracks or microcracks. Concrete failure behavior in compressive regime is governed by both, fracture energy releases in active microcracks and material degradation in between these cracks. Moreover, the width of the characteristic dimension of the material volume participating in the energy dissipation process in the form of cracks opening and material degradation mechanisms, increases with the acting confining pressure, as can be seen in Hurlbut (1985), van Geel (1998), Sfer et al. (2002), Lu (2005), van Mier (1984).

This complex variation from brittle to ductile failure mode in quasi-brittle materials like concrete requires special provisions for constitutive theories to accurately describe the whole spectrum of possible failure mechanisms. As the involved complexity goes beyond the capability of every known material formulation, a combination of constitutive theories is required. In this regard, a recent proposal by the authors, Vrech and Etse (2009), refers to a

* Corresponding author at: Department of Engineering, University of Buenos Aires, Argentina. Tel.: +54 381 4245027.
E-mail addresses: svrech@herrera.unt.edu.ar (S.M. Vrech), getse@herrera.unt.edu.ar (G. Etse).
[1] Maipu 780, 4000 Tucuman, Argentina.

0020-7683/$ - see front matter © 2012 Elsevier Ltd. All rights reserved.
doi:10.1016/j.ijsolstr.2012.02.009

thermodynamically consistent constitutive formulation that combines both fracture energy and gradient concepts. The so-called fracture energy and gradient-based model includes isotropic hardening and softening formulations. In the hardening regime the material model is fully local. To account for the increasing ductility with the confining pressure the hardening rule is formulated as a dependent function of the first invariant of the stress tensor. In the softening regime it is considered that two independent processes contribute to the material decohesion: the degradation process of the continuum in between cracks and the crack opening process (single or multiple). The first one is described by means of a non-local gradient-based plasticity formulation with pressure dependent characteristic length to appropriately describe the variable shear band width with the acting confinement. The crack opening process is described by a fracture energy-based plasticity formulation similarly to the proposal by Etse and Willam (1994).

Given the extensive use of the smeared-crack theory for constitutive modelling of engineering materials, one of the most challenging and relevant research activities in computational mechanics are those related to the analysis of the failure mode predicted by the material theories (localized or diffuse) for the whole spectrum of maximal stress states. Particularly important is the evaluation of brittle or localized failure modes that in the framework of continuums models are described by means of discontinuous bifurcations or jumps in the velocity gradients. In this regard, there were several analytical and geometrical attempts to capture the onset of localization and to determine both direction and amplitude of the related cracks or shear bands. After the original works by Hadamard (1903), Nadai (1950), Thomas (1961), Hill (1962), Rudnicki and Rice (1975), many authors studied the problem in a systematic manner. They basically developed mathematical conditions and indicators that signalize the initiation of localized failure modes in the form of discontinuous bifurcation, see a.o. Sobh (1987), Perić (1990), Ottosen and Runesson (1991), Willam and Etse (1990), Rizzi et al. (1995), Etse and Willam (1999), Pijaudier-Cabot and Benallal (1993), Jirásek and Rolshoven (2009a,b), Etse and Vrech (2006), Vrech and Etse (2006), Arslan et al. (2007). In this work, analytical and geometrical methods are developed to evaluate the predictions of localized failure modes and the transition from brittle to ductile failure provided by the thermodynamically consistent gradient and fracture energy-based plasticity theory for cohesive-frictional materials like concrete as proposed by Vrech and Etse (2009) when it is combined with the Leon–Drucker Prager (LDP) maximum strength criterion. The gradient-dependent elastoplastic localization properties are casted in the form of an elliptical envelope condition in the $\sigma_N - \tau_N$ coordinates of Mohr, as described in Benallal and Comi (1996) and Liebe and Willam (2001). Thereby, the tangency condition between the localization ellipse and the major principal circle defines the existence of localized failure mode and the corresponding critical directions. The results of the localization analysis demonstrate the capability of the thermodynamically consistent gradient and fracture energy dependent elastoplastic LDP model to realistically predict both brittle and ductile failure modes of concrete when the governing stress state varies from the tensile and low confinement regime to the high confinement one. The localization analysis results are complemented with model predictions of the gradient characteristic length for different stress conditions to demonstrate the strong dependence of the acting confinement on the zone size, where the inelastic and fracture processes is located.

2. Thermodynamically consistent gradient-dependent elastoplasticity

Following the thermodynamically consistent gradient-regularized material theory for small strain kinematics by Svedberg and Runesson (1997), the free energy density Ψ can be additively decomposed into three components as follows: elastic, *local* and *non-local* plastic. Considering isotropic plasticity, the non-local effects are only restricted to the scalar hardening/softening variable κ.

As deduced in Svedberg (1999), the constitutive equation for the stress tensor $\boldsymbol{\sigma}$, obtained from the Coleman's relations, results

$$\boldsymbol{\sigma} = \rho \frac{\partial \Psi}{\partial \boldsymbol{\varepsilon}}, \quad \boldsymbol{\sigma} = \boldsymbol{E}^e : \boldsymbol{\varepsilon}^e \tag{1}$$

being $\boldsymbol{\varepsilon}$ the strain tensor and $\boldsymbol{E}^e$ the fourth order elastic operator. The dissipative stress within the continuum is defined as the addition of the *local* and *non-local* plastic dissipative stresses, $K = K^p + K^g$, with

$$K^p = -\rho \frac{\partial \Psi^p}{\partial \kappa} \quad \text{and} \quad K^g = \nabla \cdot \left[\rho \frac{\partial \Psi^g}{\partial (\nabla \kappa)} \right] \tag{2}$$

while the dissipative stress on the boundary $\partial\Omega$ results

$$K^{(g,b)} = -\boldsymbol{m} \cdot \rho \frac{\partial \Psi^g}{\partial (\nabla \kappa)} \tag{3}$$

with $\boldsymbol{m}$ the (outward) normal to $\partial\Omega$.

The evolution equations of the strains tensor $\dot{\boldsymbol{\varepsilon}}^p$ and state variable $\dot{\kappa}$, are

$$\dot{\boldsymbol{\varepsilon}}^p = \dot{\lambda} \frac{\partial \Phi^*}{\partial \boldsymbol{\sigma}} \quad \text{and} \quad \dot{\kappa} = \dot{\lambda} \frac{\partial \Phi^*}{\partial K} \tag{4}$$

being $\dot{\lambda}$ the rate of the plastic parameter and $\Phi^* = \Phi^*(\boldsymbol{\sigma}, K)$ the dissipative potential which turns $\Phi = \Phi(\boldsymbol{\sigma}, K)$, the convex yield function, in case of associated plasticity.

3. Elastoplastic LDP model based on gradient theory and fracture energy

In this section the thermodynamically consistent gradient-dependent model based on the LDP failure criterion, as proposed by Vrech and Etse (2009), is summarized.

The LDP failure criterion is

$$\Phi(p^*, \rho^*) = \frac{3}{2}\rho^{*2} + m_0 \left(\frac{\rho^*}{\sqrt{6}} + p^* \right) - c_0 = 0 \tag{5}$$

whereby the Haigh–Westergaard coordinates

$$p^* = \frac{I_1}{3 f_c'}, \quad \rho^* = \frac{\sqrt{2 J_2}}{f_c'} \tag{6}$$

where introduced, being I_1 the first invariant of the stress tensor and J_2 the second invariant of the deviatoric stress tensor.

The frictional parameter calibrated in terms of the uniaxial tensile and compression strengths f_t' and f_c', respectively, results

$$m_0 = \frac{3}{2} \frac{\left(f_c'^2 - f_t'^2 \right)}{f_c' f_t'} \tag{7}$$

while the cohesion is $c_0 = 1$.

Fig. 1 compares the LDP strength criterion for axisymmetric state with the normalized peak stresses of concrete obtained from experimental tests. The LDP criterion overestimates the strength of concrete in the tensile meridian (i.e. when the Lode angle equals zero). Nevertheless its overall accuracy is acceptable in view of the associated simplicity as it only depends on two stress invariants.

3.1. Yield condition

Loading surface in hardening and softening regimes is expressed as

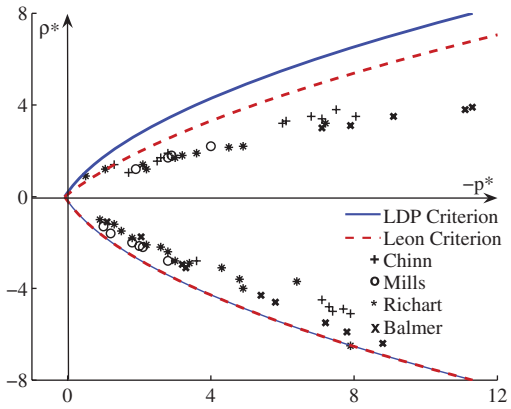

Fig. 1. Comparison of LDP strength criterion against triaxial test data on concrete.

$$\Phi(p^*,\rho^*,K_h,K_s)=\frac{3}{2}\rho^{*2}+m_0\left(\frac{\rho^*}{\sqrt{6}}+p^*\right)-K_hK_s=0 \tag{8}$$

The evolution of the yield surfaces in the pre-peak regime is controlled by the variation of the hardening dissipative stress $K_h^o \leqslant K_h \leqslant 1$, while the softening dissipative stress remains constant $K_s = 1$. A local and pressure-dependent inelastic hardening formulation is considered for the LDP model, as can be observed in Vrech and Etse (2009). When $K_h = 1$ the LDP criterion for concrete strength is reached. Under monotonic loading beyond peak stress the softening regime is activated. The strength degradation during the post-peak process is controlled by the decay of the softening dissipative stress $1 \geqslant K_s \geqslant 0$ while $K_h = 1$ remains constant.

3.2. Isotropic softening law

It is considered that the instantaneous concrete strength in softening regime results from a parallel mechanism between two components: the strength to start or further develop fracture processes K_{sf}^p, and the strength to start or further develop damage processes in the continuum material located in between active cracks K_{sc}^g. The considered mechanism controlling the strength degradation process in the post-peak regime can be mathematically expressed as

$$K_s(\kappa_s,\nabla\kappa_s)=K_{sf}^p(\kappa_s)+K_{sc}^g(\nabla\kappa_s) \tag{9}$$

being κ_s the softening state variable, the only one of non-local character, and $\nabla\kappa_s$ its spatial gradients.

3.2.1. Fracture energy-based softening law

The evolution law of the local softening dissipative stress is, see Vrech and Etse (2009)

$$\dot{K}_{sf}^p=\alpha_f\exp(-\alpha_f\lambda),\quad \alpha_f=5\frac{h_f(p^*)}{u_r}\|\langle\boldsymbol{m}_l\rangle\| \tag{10}$$

being u_r the maximum crack opening displacement in mode I type of failure and h_f the fracture characteristic length that defines the separation between cracks or microcracks. This measure represents the high of an equivalent elastoplastic continuum, obtained through the homogenization process of the released fracture energy in a discontinuous of the same size, similarly to the fracture energy-based plasticity models by Willam et al. (1985) and Etse and Willam (1994). In quasi-brittle materials like concrete the distance between microcracks strongly depends on the type of fracture as well as on the acting confining pressure.

The Mc Auley brackets in Eq. (10) indicate that only tensile principal plastic strains contribute to the energy density during fracture evolution processes.

3.2.2. Gradient-based softening law

The non-local dissipative stress in softening results

$$\dot{K}_{sc}^g=-[l_c(p^*)]^2H_{sc}^g\nabla^2\dot{\lambda} \tag{11}$$

being $\nabla^2\dot{\lambda}$ the second derivative of the plastic parameter rate, H_{sc}^g the scalar gradient modulus and l_c the gradient plasticity characteristic length. In quasi-brittle materials like concrete l_c strongly depends on the acting confining pressure during softening process. This dependence is mathematically defined by Vrech and Etse (2009) as

$$l_c(p^*)=\begin{cases}0 & \text{if } p^*\geqslant 0;\\ 0.5l_{c,m}\left[1+\sin\left(2p^*-\frac{\pi}{2}\right)\right] & \text{if } -1.5\leqslant p^*<0;\\ l_{c,m} & \text{if } p^*<-1.5.\end{cases} \tag{12}$$

being $l_{c,m}$ the maximum value of l_c. Thereby it is assumed that l_c equals the maximum aggregate size $l_{c,i}$ when $p^* = -0.33$, i.e. when the confining pressure equals f_c' corresponding to the case of the uniaxial compression test.

Note that when the characteristic length based on gradient plasticity l_c turns zero in the low confinement regime, see Eq. (12), the strength degradation process is fully controlled by the fracture energy-based mechanism. In this way, the diffusion of failure that characterizes the predictions of gradient plasticity-based material theories is suppressed and the strong localization of concrete failure in the low confinement regime should be able to be reproduced. This will be investigated in Section 6 related to localization analysis with the LDP fracture energy and gradient-based model. It should be noted that when $l_c = 0$ all eventual localized failure modes predicted by the model are related discontinuous bifurcation and, therefore, to losses of the well-posedness of the involved boundary value problem.

Traditionally, the gradient internal length has been imposed with the aim to lead dimensional stability, see a. o. Vardoulakis and Aifantis (1991), Sluys et al. (1993), Pamin (1994), Svedberg (1999). Actually, according to Svedberg and Runesson (1997) there are three possible interpretations of l_c:

- a convenient dimensional parameter in order to $\overline{H}$ and $\overline{H}^g$ will get the same dimension,
- a physical entity that defines a characteristic measure of the microstructure, and
- a parameter that numerically stabilizes the non-local constitutive theory.

In this paper l_c is a gradient characteristic length that: (i) homogenizes the dimensions of $\overline{H}$ and $\overline{H}^g$, (ii) determines the energy dissipation zone depending on the microstructure, or (iii) stabilizes the algorithmic solution process, according to the mathematical, physical or numerical viewpoint, respectively.

Moreover, in recent years several authors have investigated the physical aspects of the characteristic length corresponding to granular materials, see a.o. Voyiadjis et al. (2005) and Arslan and Sture (2008).

3.2.3. Non-associated flow rule

To reduce excessive dilatation of concrete during fracture process in the low confinement regime, a limited non-associated flow rule was defined for the constitutive model, whereby only the volumetric flow is non-associated. The plastic potential is defined as

$$\Phi^*(p^*,\rho^*,K_h,K_s)=\Phi(p^*,\rho^*,K_h,K_s)+m_0p^*(\eta-1)=0 \tag{13}$$

being η the degree of volumetric non-associativity that varies between $0 \leqslant \eta \leqslant 1$. Fig. 2 shows the effect of the non-associated rule in the dilatation performance of model predictions of failure behavior in the uniaxial compression test.

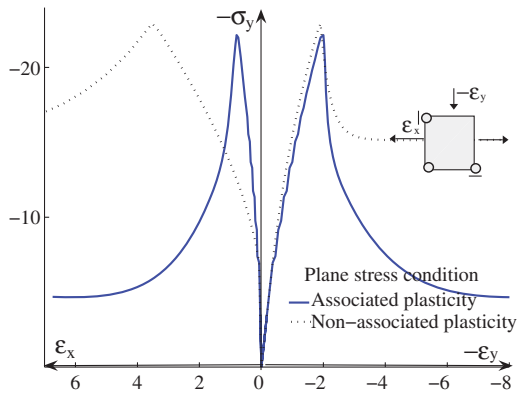

Fig. 2. Comparison of the associated and non-associated rules of LDP model predictions in the uniaxial compression test.

4. Analytical solution for localized failure of the LDP fracture energy and gradient-based model

In the realm of the smeared crack approach, localized failure modes are related to discontinuous bifurcations of the equilibrium path, and lead to lost of ellipticity of the equations that govern the static equilibrium problem. The inhomogeneous or localized deformation field exhibits a plane of discontinuity that can be identified by means of the eigenvalue problem of the acoustic or localization tensor, see a.o. Ottosen and Runesson (1991) and Willam and Etse (1990).

Analytical solutions of the discontinuous bifurcation condition in gradient non-local continua follow from the waves propagation analysis, see Svedberg (1999).

The elastoplastic material operator can be expressed as

$$\boldsymbol{E}^{ep} = \boldsymbol{E}^{e} - \frac{1}{(h+h_g)}\boldsymbol{E}^{e} : \frac{\partial \Phi^{*}}{\partial \boldsymbol{\sigma}} \otimes \frac{\partial \Phi}{\partial \boldsymbol{\sigma}} : \boldsymbol{E}^{e} \tag{14}$$

whereby the generalized local plastic modulus h is defined as

$$h = \frac{\partial \Phi}{\partial \boldsymbol{\sigma}} : \boldsymbol{E}^{e} : \frac{\partial \Phi^{*}}{\partial \boldsymbol{\sigma}} + \overline{H}, \quad \text{with} \quad \overline{H} = H \frac{\partial \Phi}{\partial K}\frac{\partial \Phi^{*}}{\partial K} \tag{15}$$

while the *non-local* one h_g as

$$h^{g} = \overline{H}^{g}\left(\frac{2\pi l}{\delta}\right)^{2}, \quad \overline{H}^{g} = H^{g}\frac{\partial \Phi}{\partial K}\frac{\partial \Phi^{*}}{\partial K} \tag{16}$$

being δ the final localization or wave length and H and H^g the local and non-local hardening/softening modulus, respectively. Similarly, $\overline{H}$ and $\overline{H}^g$ are the thermodynamically consistent local and non-local hardening/softening modulus, respectively.

The localized failure condition of gradient-dependent elastoplasticity

$$det(\boldsymbol{Q}^{g}) = 0 \tag{17}$$

leads to the analysis of the spectral properties of the localization tensor $\boldsymbol{Q}^g$ defined as

$$\boldsymbol{Q}^{g} = \boldsymbol{Q} - \frac{1}{h+h^{g}}\boldsymbol{a}^{*} \otimes \boldsymbol{a} \tag{18}$$

being $\boldsymbol{Q}$ the elastic localization tensor

$$\boldsymbol{Q} = \boldsymbol{n}_l \cdot \boldsymbol{E}^{e} \cdot \boldsymbol{n}_l \tag{19}$$

and $\boldsymbol{n}_l$ the normal direction to the discontinuity surface.

The smallest eigenvalue of $\boldsymbol{Q}^g$ with respect to the metric defined by $[\boldsymbol{Q}]^{-1}$ is

$$\lambda^{(1)} = 1 - \frac{\boldsymbol{a}(\boldsymbol{n}_l)\cdot[\boldsymbol{Q}(\boldsymbol{n}_l)]^{-1}\cdot\boldsymbol{a}^{*}(\boldsymbol{n}_l)}{h+h^{g}} = 0 \tag{20}$$

with the vectors $\boldsymbol{a}^*$ and $\boldsymbol{a}$ defined as

$$\boldsymbol{a}^{*} = \boldsymbol{n}_l \cdot \boldsymbol{E}^{e} : \frac{\partial \Phi^{*}}{\partial \boldsymbol{\sigma}} \quad , \quad \boldsymbol{a} = \frac{\partial \Phi}{\partial \boldsymbol{\sigma}} : \boldsymbol{E}^{e} \cdot \boldsymbol{n}_l \tag{21}$$

By replacing Eqs. 15, 16 and 21 in Eq. (20), results

$$\mathcal{H} + \frac{\partial \Phi}{\partial \boldsymbol{\sigma}} : \boldsymbol{E}^{e} : \frac{\partial \Phi^{*}}{\partial \boldsymbol{\sigma}} - \boldsymbol{a}\cdot[\boldsymbol{Q}]^{-1}\cdot\boldsymbol{a}^{*} = 0 \tag{22}$$

with

$$\mathcal{H} = \overline{H}_c^{g}\left(\frac{2\pi l_c}{\delta}\right)^{2} + \overline{H}_c \tag{23}$$

The localization condition in Eq. (22) serves as a basis for analytical and numerical evaluations of the most critical (maximum) hardening parameter $\overline{H}_c(\boldsymbol{n}_l) = max[\overline{H}(\boldsymbol{n}_l)]$ and $\overline{H}_c^{g}(\boldsymbol{n}_l) = max[\overline{H}^{g}(\boldsymbol{n}_l)]$ for discontinuous bifurcation and of their associated localization directions $\boldsymbol{n}_l$, corresponding to any possible stress history.

In the particular case of local elastoplasticity, when $l_c \to 0$, the localization condition $det(\boldsymbol{Q}^{ep}) = 0$ turns

$$\overline{H}_c + \frac{\partial \Phi}{\partial \boldsymbol{\sigma}} : \boldsymbol{E}^{e} : \frac{\partial \Phi^{*}}{\partial \boldsymbol{\sigma}} - \boldsymbol{a}\cdot[\boldsymbol{Q}]^{-1}\cdot\boldsymbol{a}^{*} = 0 \tag{24}$$

General explicit solutions for the critical hardening modulus and related localization directions for classical plasticity were developed by Ottosen and Runesson (1991) in case of tridimensional stress states, and by Perić (1990) in case of plane states. Analytical solutions for discontinuous bifurcation of quasi-brittle materials were developed by Etse (1992a) and Etse (1992b) under consideration of a local elastoplastic model for concrete. As demonstrated by Vrech and Etse (2006) gradient-based elastoplastic theories with non-local effects limited to the state variables are unable to fully regularize softening behavior and lead to similar localized failure modes of their associated local formulations when:

Case 1: Wave length $\delta \to \infty$, resulting $h_g = 0$, i.e. the local plasticity case is recovered. Then, Eq. (24) turns the valid localization condition.

Case 2: The adopted hardening/softening local modulus satisfies the condition $\overline{H} < \overline{H}_c$. Then

$$\overline{H}_c = \overline{H} + \overline{H}_c^{g}\left(\frac{2\pi l_c}{\delta}\right)^{2} \tag{25}$$

and the critical gradient modulus verifies

$$\overline{H}_c^{g} = (\overline{H}_c - \overline{H})\left(\frac{\delta}{2\pi l_c}\right)^{2} \tag{26}$$

Notice in this last equation, that adopting $\overline{H}^{g} < \overline{H}_c^{g}$ the regularization properties of the gradient theory are suppressed, i.e. localized failure modes are obtained, allowing brittle-ductile failure transitions.

5. Geometrical method for discontinuous bifurcation in gradient-based elastoplastic LDP model

In this section, the geometrical method for localization analysis of the thermodynamically consistent gradient and fracture energy-based LDP model is developed. The approach follows the original proposal by Benallal (1992), which was further developed by Pijaudier-Cabot and Benallal (1993), Benallal and Comi (1996), Liebe and Willam (2001) for classical plasticity, and by Etse and Vrech (2006), Vrech and Etse (2006) for non-local gradient-based plasticity.

The localization condition in Eq. (22) defines an ellipse

$$\frac{(\sigma-\sigma_0)^2}{A^2}-\frac{\tau^2}{B^2}=1 \tag{27}$$

in the $\sigma-\tau$ Mohr's coordinates

$$\sigma=\boldsymbol{n}_l\cdot\boldsymbol{\sigma}\cdot\boldsymbol{n}_l,\quad s=\boldsymbol{n}_l\cdot\boldsymbol{S}\cdot\boldsymbol{n}_l \tag{28}$$

$$\tau=(\boldsymbol{n}_l\cdot\boldsymbol{S})\cdot(\boldsymbol{n}_l\cdot\boldsymbol{S})-(\boldsymbol{n}_l\cdot\boldsymbol{S}\cdot\boldsymbol{n}_l)^2 \tag{29}$$

being $\boldsymbol{S}$ the deviatoric stress tensor and $\boldsymbol{n}_l$ the normal to the plane, where the Mohr components are evaluated. The localization ellipse and Mohr's circle parameters are shown in Fig. 3.

To obtain the ellipse's center σ_0 and the horizontal and vertical half axes A and B corresponding to the gradient-dependent non-associated LDP model, the gradient functions

$$\boldsymbol{n}=\frac{\partial\Phi}{\partial\boldsymbol{\sigma}}=a_1\boldsymbol{S}+a_2\boldsymbol{I}\quad,\quad \boldsymbol{m}=\frac{\partial\Phi^*}{\partial\boldsymbol{\sigma}}=a_1\boldsymbol{S}+a_3\boldsymbol{I} \tag{30}$$

are involved with

$$a_1=3f_t'+\frac{m_0}{\sqrt{6}\rho}f_t'f_c' \tag{31}$$

$$a_2=\frac{m_0}{3}f_t'f_c' \tag{32}$$

$$a_3=\eta a_2 \tag{33}$$

By adopting for the elastic tensor $\boldsymbol{E}^e$ the form

$$\boldsymbol{E}^e=2G\boldsymbol{I}_4+\Lambda\boldsymbol{I}\otimes\boldsymbol{I} \tag{34}$$

with the Lame's parameters

$$\Lambda=\frac{E\nu}{(1+\nu)(1-2\nu)},\quad G=\frac{E}{2(1+\nu)} \tag{35}$$

the traction vectors in Eq. (21) can be rewritten as

$$\boldsymbol{a}^*=2a_1G\boldsymbol{n}_l\cdot\boldsymbol{S}+a_3\frac{E}{(1-2\nu)}\boldsymbol{n}_l \tag{36}$$

$$\boldsymbol{a}=2a_1G\boldsymbol{n}_l\cdot\boldsymbol{S}+a_2\frac{E}{(1-2\nu)}\boldsymbol{n}_l \tag{37}$$

Replacing $\boldsymbol{E}^e$ from Eq. (34) in Eq. (19), we obtain

$$\boldsymbol{Q}=G\left[\boldsymbol{I}-\frac{1}{(1-2\nu)}\boldsymbol{n}_l\otimes\boldsymbol{n}_l\right] \tag{38}$$

and its inverse results

$$[\boldsymbol{Q}]^{-1}=\frac{1}{G}\left[\boldsymbol{I}-\frac{1}{2(1-\nu)}\boldsymbol{n}_l\otimes\boldsymbol{n}_l\right] \tag{39}$$

The maximum hardening/softening parameter $\overline{H}_c$ and the critical directions θ_c for localization, according Fig. 3, are obtained when the Mohr circle of stresses

$$(\sigma-\sigma_c)^2+\tau^2=R^2 \tag{40}$$

contacts the elliptical localization envelope. The center and radius of the Mohr circle in Eq. (40), are

$$\sigma_c=\frac{\sigma_1+\sigma_3}{2}\quad\text{and}\quad R=\frac{\sigma_1-\sigma_3}{2} \tag{41}$$

with σ_1 and σ_3, the major and minor principal stresses, respectively. The center σ_0 and half axes A and B of the localization ellipse in Eq. (27) are defined by

$$\sigma_0=\frac{1}{3}I_1-\frac{(a_2+a_3)}{2a_1}\frac{(1+\nu)}{(1-2\nu)} \tag{42}$$

$$B^2=\frac{\mathcal{H}}{4Ga_1^2}+J_2+\frac{a_2a_3}{a_1^2}\frac{(1+\nu)}{(1-\nu)}+\frac{(a_2+a_3)^2}{8a_1^2}\frac{(1+\nu)^2}{(1-2\nu)(1-\nu)} \tag{43}$$

$$A^2=2\frac{(1-\nu)}{(1-2\nu)}B^2 \tag{44}$$

According to Liebe (1998) three different failure modes may be distinguished depending on the contact points location: mode I, mode II and mixed mode. Fig. 4 illustrates the interrelationship between the radius R of the Mohr's circle and the curvature of the localization ellipse ρ^e for the three different failure modes, with

$$\rho^e_{min}\leqslant\rho^e\leqslant\rho^e_{max},\quad\text{being}\quad\rho^e_{min}=\frac{B^2}{A},\quad\rho^e_{max}=B \tag{45}$$

The critical failure directions θ_c for localization, obtained from the tangential contact between the elliptical localization envelope of Eq. (27) and the major Mohr's circle of Eq. (40), are expressed as

$$\tan^2(\theta_c)=\frac{R-(\sigma_c-\sigma_0)/(d^2-1)}{R+(\sigma_c-\sigma_0)/(d^2-1)};\quad d^2=\frac{A^2}{B^2} \tag{46}$$

Remark. In the particular case of classical elastoplasticity the differential Eq. (22) turns

$$\overline{H}_c(\boldsymbol{n}_l)=-\frac{\partial\Phi}{\partial\boldsymbol{\sigma}}:\boldsymbol{E}^e:\frac{\partial\Phi^*}{\partial\boldsymbol{\sigma}}+\boldsymbol{a}\cdot[\boldsymbol{Q}^e]^{-1}\cdot\boldsymbol{a}^* \tag{47}$$

therefore, the parameter B^2 representing the vertical axis of the ellipse in Eq. (27) takes now the form

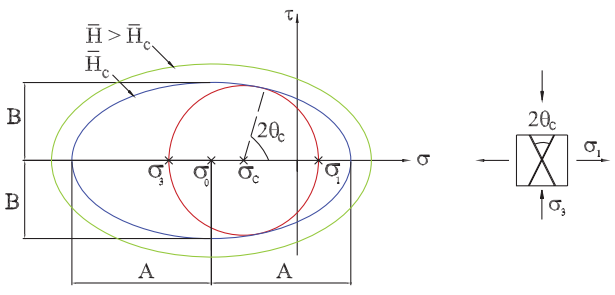

Fig. 3. Mohr circle and localization ellipse.

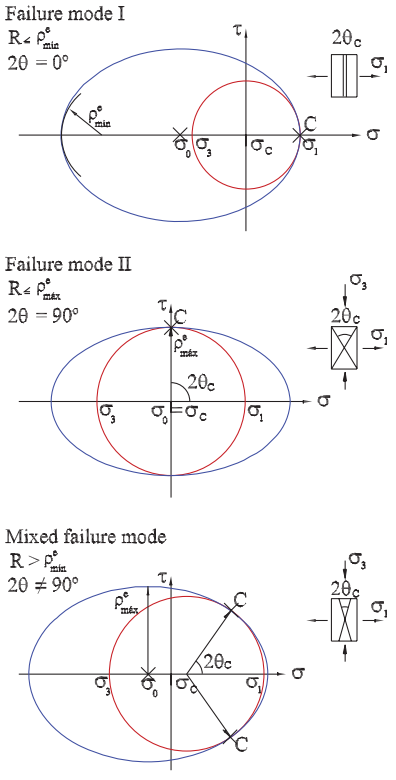

Fig. 4. Failure modes and localization envelope of Mohr's circle.

$$B^2 = \frac{\overline{H}_c}{4Ga_1^2} + J_2 + \frac{a_2 a_3}{a_1^2}\frac{(1+\nu)}{(1-\nu)} + \frac{(a_2+a_3)^2}{8a_1^2}\frac{(1+\nu)^2}{(1-2\nu)(1-\nu)} \quad (48)$$

6. Localization analysis for the gradient and fracture energy-based thermodynamically consistent LDP model

The localization analysis in this section considers both plane strain and plane stress conditions. In Section 6.1 the localization properties of the thermodynamically consistent LDP model are analyzed for the particular plane strain state when $\sigma_z = \nu(\sigma_x + \sigma_y)$. Section 6.2 refers to the localization analysis in plane stress condition. The following material properties are considered

Elastic modulus – E = 19305.3 MPa
Poisson's ratio – $\nu = 0.2$
Compressive strength – $f_c' = 22.0$ MPa
Tensile strength – $f_t' = 2.7$ MPa
Initial internal length – $l_{c,i} = 25.0$ mm
Maximal internal length – $l_{c,m} = 110.0$ mm
Gradient modulus – $H^g = 470.70$ MPa

Previously to the localization analysis it is illustrative to see the differences of model predictions in plane strain and plane stress conditions. Fig. 5 shows the predictions of uniaxial compression tests in both plane conditions. Due to the induced out-of-plane stress, the plane strain condition leads to overestimation of the material strength and to a more ductile failure behavior.

6.1. Localization analysis plane strain state

Fig. 6 illustrates the variation of the normalized localization indicator $det(Q^g)/det(Q)$ of the LDP gradient and fracture energy-based material along its maximal strength criterion defined in terms of the normalized first and second Haigh–Westergaard stress coordinates and under plane strain conditions. The gradient internal length l_c follows Eq. (12). As can be observed from Fig. 6, a clear and realistic transition point from ductile or diffuse failure modes to brittle or localized ones is predicted by the model when the confining pressure decreases towards the low confinement and tensile regimes. This transition is signalized by the appearance of null values of the normalized localization indicator corresponding to discontinuous bifurcation.

Fig. 7 shows the evolution of the normalized critical hardening parameter $\overline{H}_c/E$ along the maximum strength surface in the σ_1/f_c' and σ_2/f_c' plane and under plane strain conditions. In this figure $\overline{H}_c/E$ is depicted in the normal direction to the strength surface

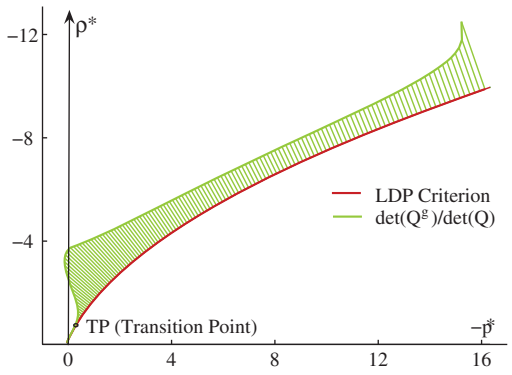

Fig. 6. Evolution of the localization indicator in normal direction to the LDP maximal strength criterion. Plain strain state.

in outward direction when it's positive. It can be observed that the plane strain conditions strongly limits the region, where localized failure modes may occur (between points A and B). It is very illustrative to evaluate the influence of the eccentricity $e = \rho_t/\rho_c$ of the maximum strength surface on the localized failure indicator. Figs. 8 and 9 show the maximum strength surfaces for $e = 1$ (Leon–Drucker Prager strength criterion), $e = 0.8$ and $e = 0.5$ in the σ_1/f_c' vs σ_2/f_c' plane under plane strain conditions. The reduction of the eccentricity, i.e. the increase of the third invariant influence in the yield condition destabilizes the failure modes as the length of

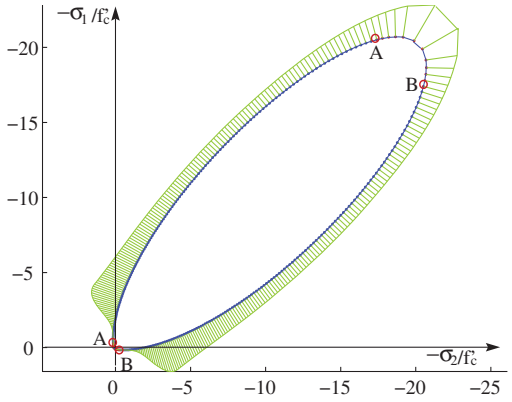

Fig. 7. Variation of the normalized critical hardening modulus along LDP maximal strength criterion in plane strain state. $\overline{H}_c/E$ is indicated in normal direction to the maximal strength surface.

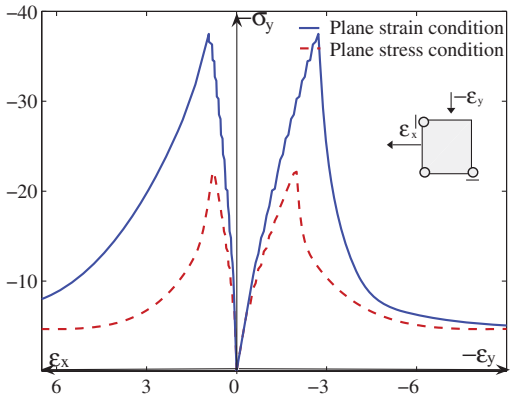

Fig. 5. Uniaxial compression tests LDP model predictions in plane strain and plane stress conditions.

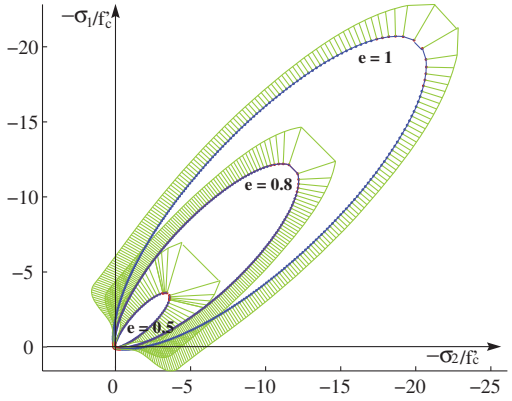

Fig. 8. Influence of the eccentricity $e = \rho_t/\rho_c$ on the evolution of the normalized critical hardening modulus $\overline{H}_c/E$ in plane strain conditions.

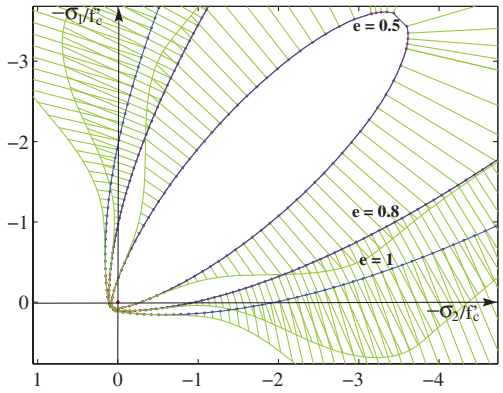

Fig. 9. Amplification of Fig. 8. Influence of the eccentricity $e = \rho_t/\rho_c$ on the evolution of the normalized critical hardening modulus $\bar{H}_c/E$ in plane strain conditions.

the maximal strength surface under localized failure mode, relative to the total length of this surface, significantly increases. Moreover, as can be observed in Fig. 9, more confinement is required to remain in the region of diffuse failure mode by decreasing e.

Now the localization analysis in plane strain conditions is performed by means of the geometrical method. Fig. 10a and b show the tangential condition analysis between the Mohr circle and the localization ellipse of the LDP material under consideration of the peak stresses of the uniaxial compression test (Fig. 10a) and of the simple shear and uniaxial tensile tests (Fig. 10b). With exception of the uniaxial compression test, the tangential localized failure condition is fulfilled at peak of the other two tests. In case of the simple shear test and the uniaxial tensile test, tangential condition takes place in the critical directions $\theta_{c1} = 0°$ and $\theta_{c2} = 180°$.

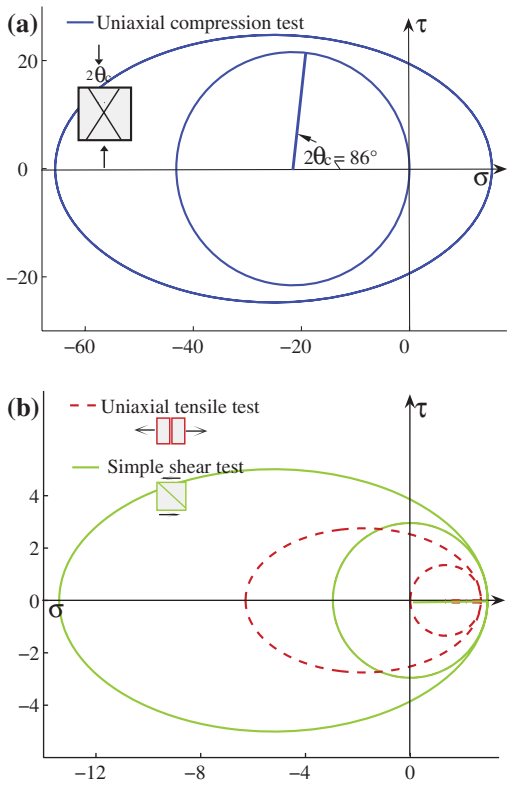

Fig. 10. Geometrical localization analysis with the LDP model at peak of (a) the uniaxial compression tests in plane strain condition and (b) the simple shear and uniaxial tensile tests in plane strain conditions.

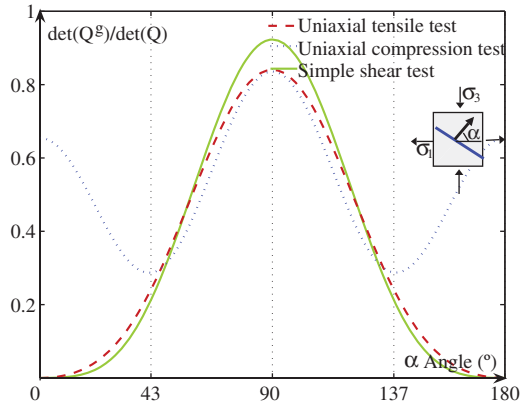

Fig. 11. Numerical localization analysis with the LDP model at peak of the simple shear, uniaxial tensile and uniaxial compression tests in plane strain state.

As a verification analysis, the normalized localization indicator is numerically evaluated at the peak stresses corresponding to the simple shear, uniaxial tensile and uniaxial compression tests under plane strain conditions and the results are depicted in Fig. 11. Both the geometrical and numerical results demonstrate that under plane strain conditions, the LDP model predicts localized or brittle failure modes in tensile and simple shear regimes while the transition to ductile failure modes takes place when the stress state moves to the low confining regime. In the uniaxial compression test the failure mode turns ductile already. Also, both the geometrical and the numerical evaluations of localized failure condition lead to the same critical angles for the discontinuity surface. It is also interesting to notice that in the uniaxial compression test under plane strain condition, the critical angles for localization or shear bands are $\theta_{c1} = 43°$ and $\theta_{c2} = 137°$. In this case the characteristic length for gradient plasticity l_c is larger than zero and equals the maximum aggregate size $l_{c,i}$. Therefore, the discontinuous bifurcation conditions are suppressed.

The influence of the increasing confining pressure in the evolution of failure modes of the LDP material under plane strain conditions is shown in Figs. 12 and 13. The first one is related to the geometrical localization analysis for the triaxial compressive tests with lateral confinements σ_1 of −0.6 MPa, −3.3 MPa and −13.2 MPa. It can be clearly observed in Fig. 12 that the increasing confinement leads to larger separations between the Mohr circle and the localization ellipse, indicating that more stable or ductile failure modes take place. The numerical analyses of localization in Fig. 13 demonstrate both the absence of discontinuous bifurcation in the high confinement regime and, moreover, the increment of the positive definition of the localization tensor as well as of the related critical localization angle with the acting confinement. In conclusion, the LDP material is able to reproduce the transition from brittle to ductile failure modes of concrete under plane strain conditions when the stress state varies from the tensile to the compressive regime with increasing confinement. The results also demonstrate the capability of the combined gradient and fracture energy-based material theory to realistically reproduce the variation of the critical localization direction with the confining pressure. These predictions agree very well with experimental observations on failure behaviors of concrete specimens.

6.2. Localization analysis in plane stress state

Fig. 14 shows the variation of the normalized localization indicator along maximum strength surface of the LDP model in plane stress state. By comparing these results with those in Fig. 6 corresponding to plane strain state it can be concluded that the lack of out-of-plane stress in case of plane stresses is responsible to considerable

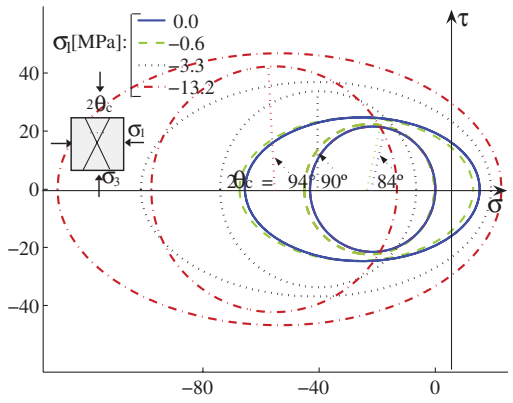

Fig. 12. Geometrical localization analysis with the LDP model at peak stress of triaxial compression tests under different confinements in plane strain state.

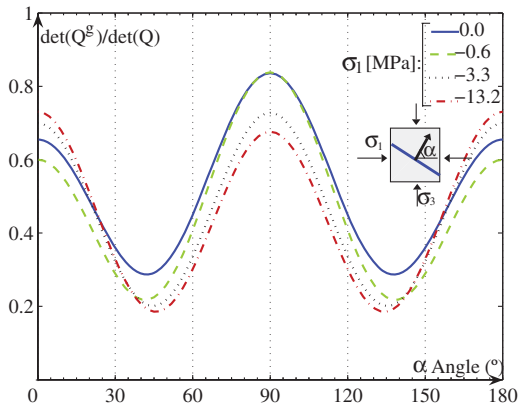

Fig. 13. Numerical localization analysis at peak of triaxial compression tests in plane strain state. LDP material model.

destabilizations of the kinematic field at peak stresses in the form of discontinuous bifurcation. Consequently, the region of the maximum strength surface related to localized failure is much larger when the material is subjected to plane stress conditions.

The variation from diffuse to localized failure regimen at peak strength of the LDP model in plane stress conditions can be observed in Fig. 15 in terms of the normalized critical hardening parameter $\overline{H}_c/E$ obtained with the analytical method for discontinuous bifurcation. In Fig. 16, the influence of the eccentricity $e = \rho_t/\rho_c$ in the evolution of the critical hardening parameter $\overline{H}_c$ is shown. It can be clearly recognized that the increasing dependence of the maximum strength surface in the third invariant (decreasing e) potentials the occurrence of localized failure in a more relevant portion of the maximal strength surface. The same effect was obtained in case of plane strain conditions.

Fig. 17 illustrates the results of the geometrical localization analysis at peak of the simple shear, uniaxial tension and uniaxial compression tests in plane stress states. Similarly to the case of plane strain condition, the uniaxial compression test is the only one that leads to diffuse failure mode as no contact between the circle of Mohr and the localization ellipse is obtained. Whereas the critical localization directions are $\theta_{c1} = 0°$ and $\theta_{c2} = 180°$ in the simple shear and in the uniaxial tensile test.

The predictions of the geometrical localization analyses related to the occurrence of discontinuous bifurcation and their associated critical directions of Fig. 17 are confirmed with the results of numerical analysis shown in Fig. 18 in terms of the determinant of the elastoplastic localization tensor normalized with that of the elastic one.

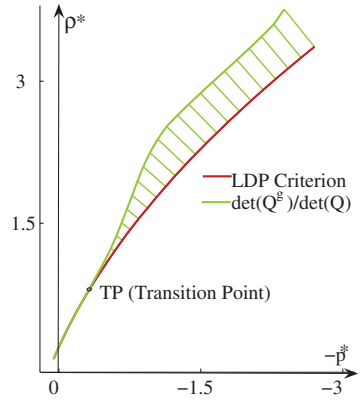

Fig. 14. Variation of the localization indicator in normal direction to the LDP maximal strength criterion. Plain stress state.

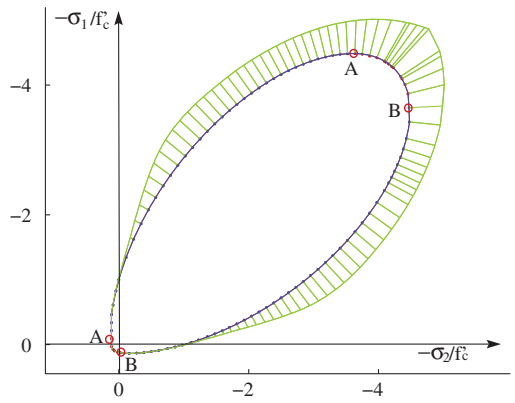

Fig. 15. Evolution of the normalized critical hardening modulus along LDP maximal strength criterion in plane stress state. $\overline{H}_c/E$ is indicated in normal direction to the maximal strength surface.

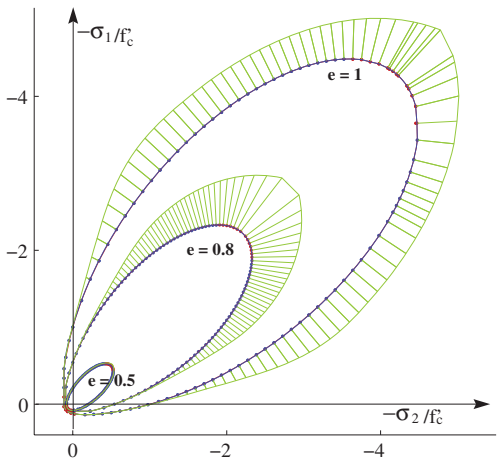

Fig. 16. Influence of the eccentricity $e = \rho_t/\rho_c$ on the evolution of the normalized critical hardening parameter $\overline{H}_c/E$ in plane stress condition.

In Figs. 19 and 20 the influence of the confinement is evaluated for three different triaxial compression tests with increasing lateral pressure. Comparing the results in Fig. 20 with those of Fig. 13 corresponding to plane strain state, it can be concluded that in plane stress condition the positive definition of the localization tensor is more sensitive to the acting confinement. However, the critical direction for localization is more sensitive to the confining pressure

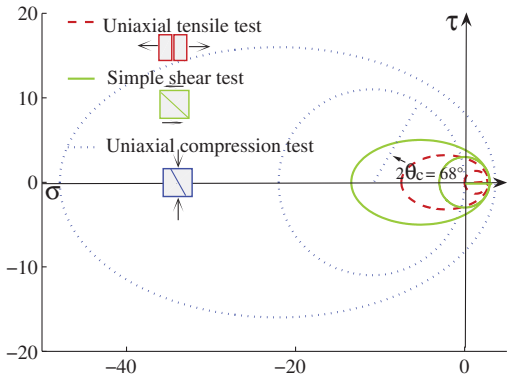

Fig. 17. Geometrical localization analysis with the LDP model at peak of the simple shear, uniaxial compression and uniaxial tensile tests in plane stress state.

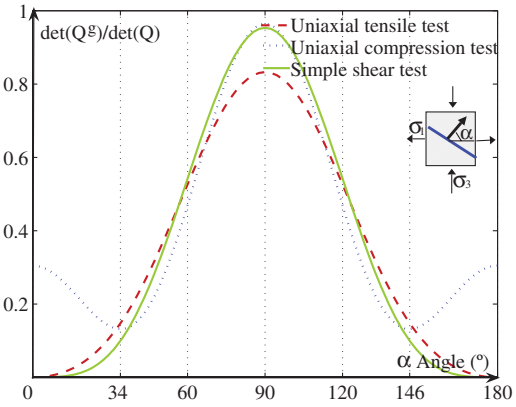

Fig. 18. Numerical localization analysis with the LDP model at peak of the simple shear, uniaxial compression and uniaxial tensile tests in plane stress state.

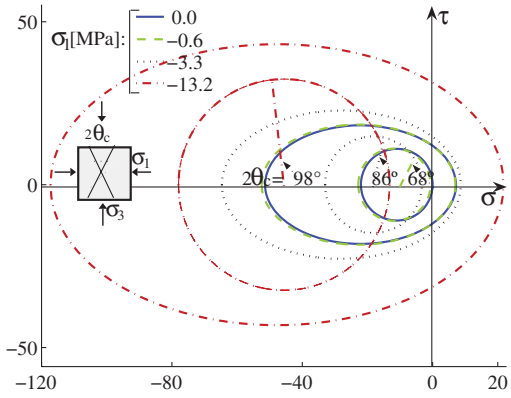

Fig. 19. Geometrical localization analysis with the LDP model at peak of triaxial compression tests under different confinements in plane stress state.

in plane strain state as the relevant increment of the out-of-plane stress that takes place in this case leads to more pronounce variations of the direction of the discontinuity surface.

Finally it is interesting to compare the performance of the localization indicator at peak stress of the uniaxial compression test in plain strain and plane stress conditions. The results in Figs. 11 and 18, respectively, demonstrate that plane strain conditions leads to more stable and ductile failure behavior as the determinant of the acoustic tensor is larger than that of the plane stress condition.

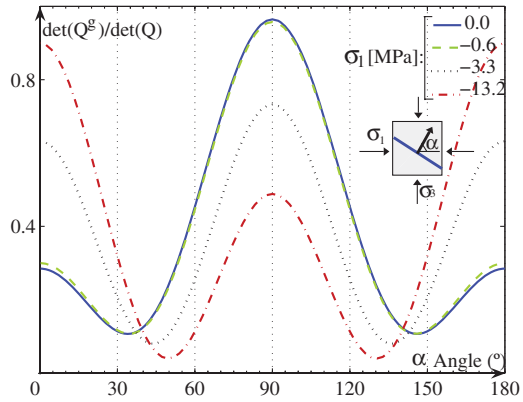

Fig. 20. Numerical localization analysis at peak of triaxial compression tests in plane stress state. LDP material model.

7. Conclusions

In this work, numerical, analytical and, particularly, geometrical procedures for localized failure evaluations in thermodynamically consistent gradient and fracture energy-based materials are presented. The constitutive theory for quasi-brittle materials like concrete proposed by the authors, see Vrech and Etse (2009), is considered together with the so-called Leon–Drucker Prager maximum strength criterion. Numerical analyses of the condition for discontinuous bifurcation are based on the evaluation of the spectral properties of the acoustic or localization tensor through the calculation of its determinant. In the analytical procedure for localized failure evaluation, explicit solutions for the critical or maximum possible hardening/softening parameter of the considered material theory are obtained, that fulfill the discontinuous bifurcation condition. Finally, in the geometrical localization method also pursued in this work, the localization ellipse in the Mohr stress coordinates is formulated for the considered selective non-local constitutive theory and then, the tangential conditions with the Mohr circle are evaluated. Both the analytical and geometrical formulations for localized failure analysis presented in this paper allow detailed evaluations of the failure mode predictions of the gradient and fracture energy-based constitutive theory for concrete. The obtained results for the localization analyses under plane strain and plane stress conditions demonstrate the capabilities of the constitutive model for concrete to reproduce diffuse failure modes in the medium and high confinement regimes while localized failure in the tensile regime. Due to the relative or limited non-locality of the constitutive theory, localized failure modes in tensile regime when the confinement pressure turns zero are related to loss of well-posedness of the boundary value problem and to discontinuous bifurcation. In this form, the well known quasi-brittle properties of concrete are realistically reproduced as well as the strong localization and unstable behavior during failure processes in the tensile regime. The results also illustrate the fundamental differences between failure modes in plane strain and plane stress conditions. The second one is more sensitive to localized failure mode in the form of discontinuous bifurcation, while the plane strain condition leads to more relevant variations of the critical localization directions.

Acknowledgements

The authors acknowledge the financial support for this work by FONCYT (Argentina agency for the promotion of research and technology) through the Grants *PICT* 1232/6, by CONICET (National

council for science and technology) through the Grant PIP 112-200801-00707 and by CIUNT (Research council of the University of Tucuman) through the Grants 26/E479.

References

Arslan, H., Sture, S., 2008. Evaluation of a physical length scale for granular materials. Comput. Mater. Sci. 42, 525–530.

Arslan, H., Sture, S., Willam, K.J., 2007. Analytical and geometrical representation of localization in granular materials. Acta Mech. 194, 159–173.

Benallal, A., 1992. On localization phenomena in thermo-elasto-plasticity. Arch. Mech. 44, 15–29.

Benallal, A., Comi, C., 1996. Localization analysis via a geometrical method. Int. J. Solids Struct. 33, 99–119.

Ehlers, W., Volk, W., 1997. On shear band localization phenomena of liquid-saturated granular elastoplastic porous solid material accounting for viscosity and micropolar solid rotations. Mech. Frict. Mater. 2, 301–320.

Etse, G., 1992a. Theoretische und numerische Untersuchung zum diffusen und lokalisierten Versagen in Beton. Ph.D. Thesis, University of Karlsruhe, Germany.

Etse, G., 1992b. Numerical failure analysis of pull-out test. Zeit. Angew. Math. Mech. 4, 158–161.

Etse, G., Vrech, S., 2006. Geometry method for localization analysis in gradient-dependent J_2 plasticity. J. Appl. Mech. 73, 1026–1030.

Etse, G., Willam, K.J., 1994. A fracture energy-based constitutive theory for inelastic behavior of plain concrete. J. Eng. Mech. 120 (9), 1983–2011.

Etse, G., Willam, K.J., 1999. Failure analysis of elasto-viscoplastic material models. J. Eng. Mech. 125, 60–69.

Guo, Z., Zhang, X., 1987. Investigation of complete stress-deformation curves for concrete in tension. ACI Mater. J. 84, 278–285.

Hadamard, J., 1903. Propagation des ondes et les equations d'Hydrodynamique. New York, Chelsea.

Hill, R., 1962. Acceleration waves in solids. J. Mech. Phys. Solids 10, 1–16.

Hurlbut, B., 1985. Experimental and Computational Investigation of Strain-Softening in Concrete. Master's thesis, University of Colorado.

Jirásek, M., Rolshoven, S., 2009a. Localization properties of strain-softening gradient plasticity models. Part I: Strain-gradient theories. Int. J. Solids Struct. 46, 2225–2238.

Jirásek, M., Rolshoven, S., 2009b. Localization properties of strain-softening gradient plasticity models. Part II: Theories with gradients of internal variables. Int. J. Solids Struct. 46, 2239–2254.

Liebe, T., 1998. Analytical and Geometrical Representation of Localization Analysis of Curvilinear Drucker Prager Elastoplasticity. Dipl. Thesis, Technical Report, University of Hanover, Germany.

Liebe, T., Willam, K.J., 2001. Localization results of generalized Drucker–Prager elastoplasticity. ASCE JEM. (127/6), 616–619.

Lu, X., 2005. Uniaxial and Triaxial Behavior of High Strength Concrete with and Without Steel Fibers. Ph.D. Thesis, New Jersey Institute of Technology.

Nadai, A., 1950. Theory of Flow and Fractory of Solids. Mc Graw, New York.

Oda, M., Kazama, M., 1988. Microstructure of shear bands and its relation to the mechanisms of dilatancy and failure of dense granular soils. Geotechnique 48, 465–481.

Ottosen, S., Runesson, K., 1991. Properties of discontinuous bifurcation solutions in elasto-plasticity. Int. J. Solids Struct. 27, 401–421.

Pamin, J. (1994). Gradient-Dependent Plasticity in Numerical Simulation of Localization Phenomena. PhD thesis, TU-Delft, The Netherlands.

Perić, D., 1990. Localized Deformation and Failure Analysis of Pressure Sensitive Granular Materials. University of Colorado, CEAE Dept., Boulder, USA.

Petersson, P.E. (1981). Crack Growth and Development of Fracture Zones in Plain Concrete and Similar Materials. Report TVBM-1006. Technical Report, Lund Institute of Technology, Sweden.

Phillips, D.V., Binsheng, Z., 1993. Direct tension tests on notched and un-notched plain concrete specimens. Mag. Conc. Res. 45, 25–35.

Pijaudier-Cabot, G., Benallal, A., 1993. Strain localization and bifurcation in a non-local continuum. Int. J. Solids Struct. 13, 1761–1775.

Planas, J., Elices, M., 1986. In: Wittmann, F.H. (Ed.), Towards a Measure of G_f: An Analysis of Experimental Results. Elsevier.

Planas, J., Elices, M., 1989. Conceptual and experimental problems in the determination of the fracture energy of concrete. In: Mihashi, H., Takahashi, H., Wittmann, F.H. (Eds.), Fracture Toughness and Fracture Energy: Test Methods for Concrete and Rock. Balkema.

Rizzi, E., Carol, I., Willam, K.J., 1995. Localization analysis of elastic degradation with application to scalar damage. J. Eng. Mech. 121-4, 541–554.

Rudnicki, J., Rice, J., 1975. Conditions for the localization of deformation in pressure-sensitive dilatant materials. J. Mech. Phys. Solids 23, 371–394.

Sfer, D., Gettu, R., Carol, I., Etse, G., 2002. Experimental study of the triaxial behavior of concrete. J. Eng. Mech. 128-2, 156–163.

Sluys, L.J., de Borst, R., Mühlhaus, M., 1993. Wave propagation, localization and dispersion in a gradient-dependent medium. Int. J. Solids Struct. 30, 1153–1171.

Sobh, N., 1987. Bifurcation Analysis of Tangential Material Operators. University of Colorado, CEAE Dept., Boulder, USA.

Svedberg, T., 1999. On the Modelling and Numerics of Gradient-Regularized Plasticity Coupled to Damage. Ph.D. Thesis, Chalmers University of Technology, Sweden.

Svedberg, T., Runesson, K., 1997. A thermodynamically consistent theory of gradient-regularized plasticity coupled to damage. Int. J. Plast. 13 (6-7), 669–696.

Thomas, T., 1961. Plastic Flow and Fracture in Solids. Academic Press, London.

van Geel, X., 1998. Concrete Behaviour in Multiaxial Compression. Ph.D. Thesis, Technische Universiteit Eindhoven, Neatherlands.

van Mier, J.G.M., 1984. Strain-Softening of Concrete under Multiaxial Loading Conditions. Ph.D. Thesis, Eindhoven University of Technology, Neatherlands.

van Mier, J.G.M., 1997. Fracture Processes of Concrete. CRC Press.

Vardoulakis, I., 1980. Shear band inclination and shear modulus of sand in biaxial tests. Int. J. Numer. Anal. Meth. Geomech. 4, 103–119.

Vardoulakis, I., Aifantis, E.C., 1991. A gradient flow theory of plasticity for granular materials. Acta Mech. 87, 197–217.

Voyiadjis, G., Alsaleh, M., Alshibli, K., 2005. Evolving internal length scales in plastic strain localization for granular materials. Int. J. Plast., 2000–2024.

Vrech, S., Etse, G., 2006. Geometrical localization analysis of gradient-dependent parabolic Drucker Prager elastoplasticity. Int. J. Plast. 22, 943–964.

Vrech, S., Etse, G., 2009. Gradient and fracture energy-based plasticity theory for quasi-brittle materials like concrete. Comput. Meth. Appl. Mech. 199, 136–147.

Willam, K.J., Etse, G., 1990. Failure assessment of the extended Leon model for plain concrete. In: SCI-C Conf., Zell and See, Austria. Pineridge Press, Swansea, UK, pp. 851–870.

Willam, K., Hurbult, B., Sture, S., 1985. Experimental and constitutive aspects of concrete failure. In: US-Japan Seminar on Finite Element Analysis of Reinforced Concrete Structures, ASCE-Special Publication, pp. 226–254.